Automatic Identification of Macular Edema in Optical Coherence Tomography Images

Gabriela Samagaio[1], Aída Estévez[4], Joaquim de Moura[1,2], Jorge Novo[1,2], Marcos Ortega[1,2]
and María Isabel Fernández[3,4,5]

[1]*Department of Computing, University of A Coruña, A Coruña, Spain*

[2]*CITIC- Research Center of Information and Communication Technologies, University of A Coruña, A Coruña, Spain*

[3]*Instituto Oftalmológico Gómez-Ulla, Santiago de Compostela, Spain*

[4]*Department of Ophthalmology, Complejo Hospitalario Universitario de Santiago, Santiago de Compostela, Spain*

[5]*University of Santiago de Compostela, Santiago de Compostela, Spain*

Keywords: Computer Aided Diagnosis, Retinal Imaging, Optical Coherence Tomography, Macular Edema.

Abstract: This paper proposes a novel system for the simultaneous identification and characterization of the three types of Macular Edema (ME) in Optical Coherence Tomography (OCT). These MEs are clinically defined, by the reference classification of the field, as: Serous Retinal Detachment (SRD), Diffuse Retinal Thickening (DRT) and Cystoid Macular Edema (CME). Our system uses multilevel image thresholding approaches to identify the SRD and CME cases and a learning approach for the DRT identification. The system provided promising results with F-Measures of 83.35% and 81.95% for the DRT and CME detections, respectively. It was also efficient in detecting all the SRD cases included in the testing image dataset. The system was able to identify individually the different types of ME on the OCT images but it was also capable to detect simultaneously the existence of the three ME cases when they appeared merged in the lower retinal layers.

1 INTRODUCTION

According to the World Health Organization, 9.6% of the European citizens are affected by blindness diseases, situation that is even worse in developing countries. As reference, in Sub-Saharan Africa, it can reach until 50% of the population. For the last ten years, cataracts have remained as the main cause of visual impairment, followed by macular disorders (WHO, 2012). One of the most relevant of them is the Macular Edema (ME), defined as intraretinal fluid accumulation that affects the central retinal vision, suffering morphological alterations in the retinal structures (Trichonas and Kaiser, 2014).

To diagnose these retinal diseases, ophthalmologists normally support their clinical evaluations in the analysis of different types of eye fundus images. One of the most widely used in this field is the OCT image modality. This technique allows a non-invasive and contactless evaluation of the *in vivo* histopathology (Helmy and Allah, 2013). Based on this image modality, in (Otani et al., 1999), a clinical classifica-

tion was established for the different types of ME that can be identified. This classification is the reference of the field, being clinically used worldwide by specialists. Intraretinal fluid accumulation was defined in three types based on clinical characteristics of the images, mainly properties as retinal thickness, reflectivity or area of the abnormalities. These three types are: Serous Retinal Detachment (SRD), Diffuse Retinal Thickening (DRT) and Cystoid Macular Edema (CME). Posteriorly, in the work of (Panozzo et al., 2004), they also characterized each type by the definition of 5 parameters: retinal thickness, diffusion, volume, morphology and epiretinal traction (Baamonde et al., 2017).

Figure 1 illustrates the presence of the three types of MEs, where the SRD and the CME cases are hyporeflective fluid regions with a specific swollen shape within the retinal layers, as described by the authors. Usually, the SRD edemas appear as a dome-shape in the outer retina while the CME typically appears as a circular shape in the inner retina, (Joussen et al., 2010). In the case of the DRT edemas, they are ty-

533

pically characterized by a "sponge-like" swelling appearance that results from the spread of fluid in the outer retina.

To diagnose these types of diseases, in the recent years, computational systems have been broadly used by ophthalmologists as useful tools that allow the diagnosis (even in early stages), treatment and monitoring of the evolution of the patients. In this field, some works based on the OCT image analysis are taking initial approaches to help and support the clinical decisions in the analysis of the ME. Therefore, some efforts have been applied in order to detect the intraretinal fluid on the OCT images, where particular characteristics are used as intensity, morphology, relative position and central and parafoveal retinal thickness (Willoughby et al., 2017; Montuoro et al., 2017). At the moment, none of the published works faced the three types of ME that appear in the macular region. As reference, in the work of (Sidibé et al., 2017), the authors proposed a method based on the Gaussian Mixture Model (GMM) to classify the OCT scans as normal and abnormal patients. Following a similar strategy, others (Montuoro et al., 2017) identified abnormal OCT images. In this case, they perform a simultaneous 3D segmentation of the retinal layers with the identification of two fluid regions as intraretinal fluid and Sub Retinal Fluid (SRF) using a graph-theoretic approach. The method of (Alsaih et al., 2017) used learning strategies in OCT retinal images in order to identify normal volumes versus volumes with ME presence. This analysis was based on the evaluation of the retinal thickening, hard exudates, intraretinal cystoid space formation, and subretinal fluid. In the case of (González et al., 2013), a method is proposed to detect the presence of cysts. A Watershed algorithm is applied within the retinal tissue in order to find all the possible regions in the image which might conform cystoid structures. Finally, in order to discard false positives, a learning strategy is applied to reduce the false positive set. The authors from (de Moura et al., 2017) proposed a method to identify the intraretinal cystoid regions, as regions of the OCT images that contain cysts. Hence, they defined a window size to analyze and extracts a set of image characteristics to determine the presence of cysts inside those regions.

In this paper, we propose a novel system to detect and characterize the intraretinal fluid as SRD, DRT and CME types, based on the clinical classification of reference in the field, the Otani classification. As indicated, to date, no other work faced completely the automatic identification of all the types of ME. To find the 3 types of ME, we firstly delimited the retinal area in the OCT images, where the intraretinal fluid forms the swollen regions. Following the Otani ME clinical characterization, we identify the presence of each type inside this region of interest.

The system will provide help in the standardization of the identification of the different types of ME, reducing the subjectivity of the ophthalmologists. Moreover, given the complexity of extraction of some ME cases, the proposed system will facilitate the doctor's work, allowing the early diagnosis and consequently the procedure with more adjusted treatments, improving the life quality of the patients.

2 METHODOLOGY

The proposed system receives, as input, an OCT retinal image centered in the macula. Firstly, the system segments automatically the retinal layers to delimit the region of interest (ROI) where the MEs are present. Inside this region, different strategies were applied to detect the 3 types of ME: SRD, DRT and CME, as illustrated in the diagram of Fig. 2.

The system was subdivided in three main steps for each ME search. Regarding SRD detection, a multi level adaptive image thresholding was used in order to find candidates with the lower intensity profiles. To discard the false positives detections, different rules based on the clinical knowledge were implemented. Hence, the candidates should have the specific relative position inside the retinal layers as well as a particular morphological shape (dome-shape). A similar strategy was used to detect the CME cases, as they also present a defined ovoid shape with a contrast with the retinal layers. An image thresholding method was used to identify CME candidates, followed by a filtering process of several morphological conditions as a way of increasing the efficiency of the proposed system. Finally, DRT edemas do not present well-defined boundaries and sufficient contrast with the surrounding tissue. In this way, a learning strategy was used to distinguish the "sponge-like" regions from the normal regions.

2.1 Retinal Layer Segmentation

Given the noisy characteristics of the input OCT images, a median filter was applied as a pre-processing step, clearing the image and preserving, simultaneously, the properties of the retinal layers in order to facilitate the posterior identifications.

In this work, 4 retinal layers were identified as they provide the correct delimitation of the regions where the different types of ME typically appear. The identified retinal layers are: Inner Limiting
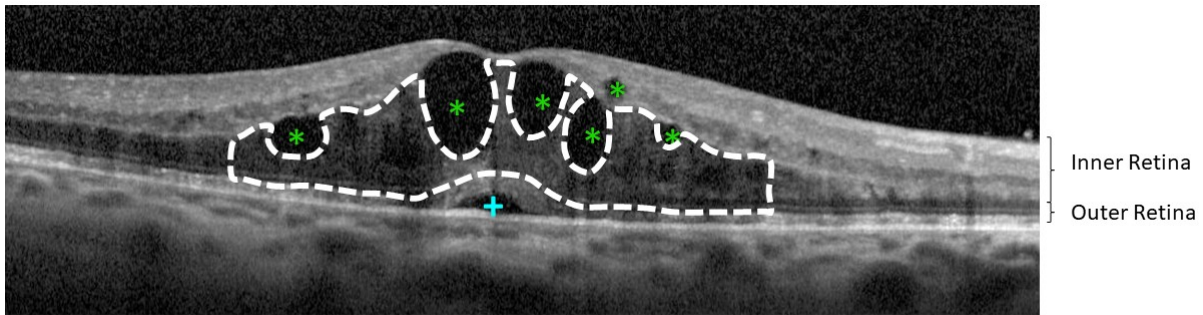
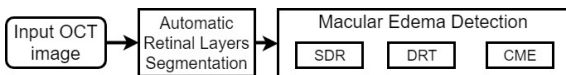Figure 1: Example of OCT retinal image with 3 types of MEs: SRD (+), CME (*) and DRT (- -).

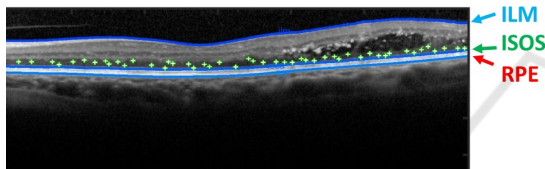Figure 2: Main methodology steps for the ME identification and characterization in SRD, DRT and CME types.

Figure 3: Example of OCT retinal image with N seeds randomly generated, near the ISOS layer.

Membrane (ILM), Outer Plexiform Layer (OPL), the junction of Inner and Outer Segments (ISOS) of the photoreceptors layers and the Retinal Pigment Epithelium (RPE).

We used an approach based on the work of (Chiu et al., 2010) to identify the indicated retinal layers. In particular, this automatic approach uses graph theory and dynamic programming to represent each OCT image as a graph of nodes, connecting optimum paths from both sides of the image. Firstly, the algorithm calculates dark-to-light gradient images, identifying adjacent layers and generating weights for the layer segmentations. The progressive identification of the main layers of the retina was found by the minimum weighted paths using the (Dijkstra, 1959) algorithm. This approach detects eight different layers in normal and healthy OCT retinal images. However, for this purpose, we adapted the method to identify 3 specific layers: ILM, ISOS and RPE.

Regarding the OPL layer, we followed a different strategy given the deteriorated conditions of the retinal layers that presents the used images of this work.

In order to solve this issue, the previous identification of the ISOS layer was used as reference for the application of region growing (Zhu and Yuille, 1996). Therefore, over this layer N initial points as seeds were randomly generated, as shown in Fig. 3. The number of seeds corresponds to a 5% of the in-

put image width. Hence, we use, as baseline, the ISOS layer to extract the region immediately over it that corresponds to the OPL layer. Using a significant number of seeds along the image we guarantee the OPL extraction even in significantly deteriorated conditions that present ME cases in advance stages.

2.2 Division in ILM/OPL and OPL/RPE Regions

As enunciated before, ME consists of the accumulation of fluid within the retinal area. However, each type of edema typically appears in particular regions inside the retinal layers that are delimited by the ILM and RPE retinal layers, as shown in Fig. 4.

According to the Otani classification, SRD and DRT edemas usually appear in the outer retina whereas CME edemas normally start manifesting in the inner retina, but they can proliferate to the outer retina in more severe pathological stages, merging with the DRT cases (Gelfand et al., 2012). Therefore, based on the previous ROI segmentation that delimits the retinal tissue, 2 sub-regions were identified: one corresponding to the inner retinal and other for the outer retina. The inner retina is comprehended between the ILM and the OPL layers, while the outer retina is delimited between the OPL and the RPE layers, as shown in Fig. 5. Thus, the detection of each type of intraretinal fluid is simplified, as the region to find each ME type is reduced.

2.3 SRD Detection

SRD edemas are typically defined as hiporeflective fluid accumulation presenting a dome-shape, with a characteristic relative position inside the retinal tissue. Therefore, the proposed system was inspired in these heuristics to automatically identify the SRD presence.

Firstly, a multi level thresholding, based on the method of (Otsu, 1979), was applied only in the ou-
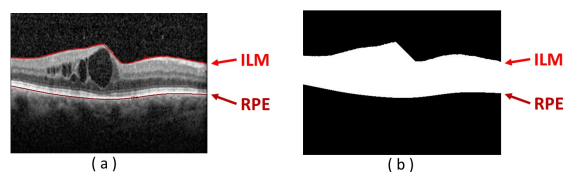
Figure 4: Example of OCT retinal image. (a) OCT image with the presence of CME edemas. (b) Binary image mask with the delimitation of the ROI between the ILM and the RPE retinal layers.
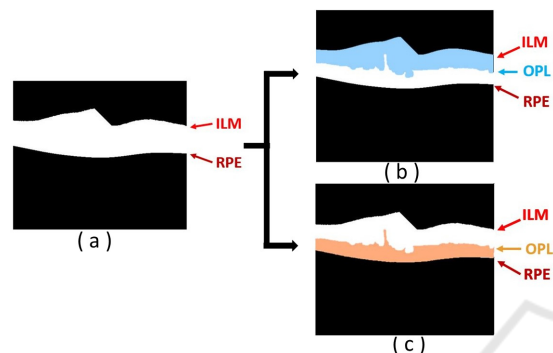

Figure 5: Inner and Outer regions of interest. (a) Entire ROI. (b) Inner retina between the ILM and the OPL retinal layers. (c) Outer retina between the OPL and RPE retinal layers.

ter retina. With this thresholding, we identify the regions with the lower intensity profiles as candidates for being SRD edema. For that, the optimal threshold was determined with the value that maximizes the separability between the intraretinal fluid regions and the retinal layers (Noma et al., 2011; Gupta et al., 2013).

Next, the objective is the removal of those candidates that do not fulfill the medical restrictions that characterize SRD edemas. Following this medical restrictions, several conditions were implemented ensuring that the system detects efficiently the SRD edemas. These conditions are:

- Relative position. This type of edemas should stay near the photoreceptors layer, (Carmona and Hernández, 2015);

- Area size, bigger than $200\mu m^2$. We selected, as reference, the area of the microcystic macular edema (Gelfand et al., 2012; Wolff et al., 2014);

- Fusiform morphology. The width that should be within an empirical range, [200 - 980]μm equivalent to [51 - 250] pixels, the typical lengths that they normally present;

- Constriction of the photoreceptors region. The SRD leads to a decrease of the region thickness delimited between the ISOS and the RPE layers in the parafoveal zone (Ooto et al., 2010). Therefore,
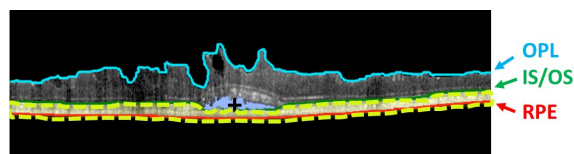

Figure 6: Example of OCT with the final ROI where was removed the region of the SRD edema (+) and the photoreceptor layer (- -).

near the fovea, we compared the mean thickness of the empirical window size and the global mean thickness of the ISOS/RPE region. The result should be less than 1 to consider the presence of candidates for being SRD edemas;

- The intensity of the area above SRD edema. This region should have a higher intensity profile when compared with the fluid region, (Ooto et al., 2010). This occurs because of part of the photoreceptors layer usually stays above the SRD edemas, as a brighter region. Hence, the mean intensity of the candidate is compared with the mean intensity of the photoreceptors layer, using the same empirical window size.

As SRD edema, if present, only appears one per image, if two or more candidates fulfill all these conditions, the system will preserve the candidate that is more centered, near the fovea.

Finally, using the SRD detection as seed, a region growing is employed to obtain the SRD segmentation as more precise as possible. This precise extraction is useful in posterior stages of the method. An example of the SRD segmentation is presented in Fig. 6.

2.4 DRT Detection

DRT or "sponge-like" edema is defined by the specialists as a retinal swelling of the macula with reduced intraretinal reflectivity. Also, this edema is typically located in the inner retina, being usually above the photoreceptor layer. Therefore, to find this type of intraretinal fluid accumulation, the proposed system searches for the DRT appearance in the OPL/RPE region, but removing the photoreceptors region and the SRD edema, when it is detected. The precise extraction of the SRD edema in the previous stage facilitates the SRD removal to calculate the new region of interest. Hence, the correction of the OPL/RPE region can be achieved accurately, resulting in a new region equivalent to the OPL/ISOS, decreasing the detection of false candidates with a more precise and restricted region to detect the DRT presence.

As this type of edema does not have a well-defined morphological shape and contour, simple methods based on image processing techniques are not sufficient
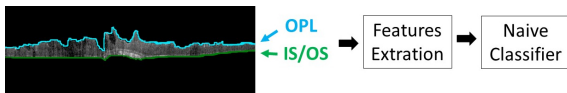
Figure 7: Example of OCT image with the new baseline on the OPL/ISOS region. The Naive Bayes classifier is trained by the feature extraction from each "espunge-like" columns.

to produce acceptable results. Therefore, in this step, a learning strategy was implemented using the Naive Bayes classifier, extracting features per column from the OPL/RPE region and identifying the DRT presence, as illustrated in the diagram of Fig. 7. We used Naive Bayes as a frequently used classifier in medical imaging approaches. The extracted features were based mainly on intensity and texture features. Moreover, another relevant property is the retinal thickness, as MEs normally produce the fluid accumulation inside the retinal layers and, therefore, the increment of their thickness (Goebel and Kretzchmar-Gross, 2002). We used this property also as an indicator of the disease presence.

Table 1 details the 18 features that were implemented to identify the DRT presence. A Sequential Forward Selection (SFS) method was applied to the feature set to reduce the array dimensionality and preserve those with the highest discriminative power.

Table 1: List of the 18 features to identify the DRT presence.

Nº of Features	Feature
1 - 6	- *Intensity Image Analysis:* Maximum, Minimum, Mean, Median, Standard-deviation and Variance
7 - 10	- *Histogram Image Analysis:* Obliquity, Kurtosis, Energy and Entropy
11 - 14	- *Mask Height Analysis:* Height of OPL/RPE region, Height of mask ILM/RPE The ratio between the heights of OPL/RPE and the ILM/RPE regions
15 - 18	- *Texture Analysis:* GLCM method: Contrast, Correlation, Energy and Homogeneity

2.5 CME Detection

Cysts typically present a low intensity profile with a significant contrast with the ILM/OPL region, where they frequently appear. A multilevel thresholding, based on the Otsu's algorithm, was also implemented in
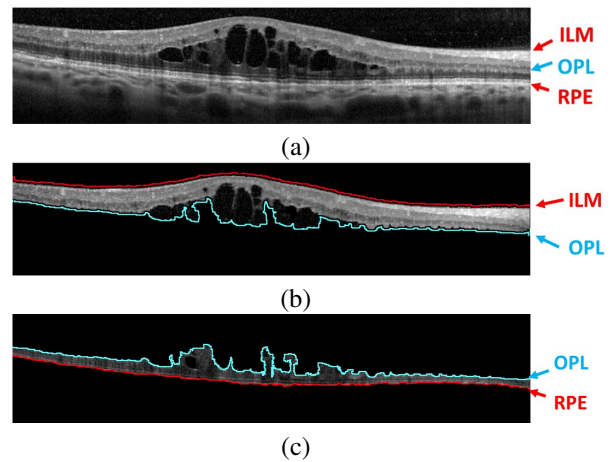

(a)

(b)

(c)

Figure 8: Example of OCT image with the presence of CMEs. (a) Input OCT retinal image. (b) CMEs represented as (*) in the ILM/OPL region. (c) CMEs (*) in OPL/RPE region with lower contrast compared to the surrounded retinal layer.

this stage, due to the contrast between the ILM/OPL region and the CMEs, identifying all the candidates for being cysts. Due to the relative high number of detected false positives, a post processing stage was implemented to preserve the real existing ones. As we can retrieve partial segmentations (even several candidates for the same cyst), we completed the segmentations using Watershed. This way, we obtain more defined reliable regions for the candidates that facilitate the posterior analysis and the false positive reduction. Hence, using as reference the clinical properties that the specialists follow to identify the cysts, we implemented a list of conditions to preserve the real CMEs from the list of candidates (Wolff et al., 2014; Joussen et al., 2010; Helmy and Allah, 2013). These conditions are listed below:

- Area size, bigger than $1\mu m^2$. To discard noisy and tissue artifacts;
- Eccentricity, should be smaller than 0.98 to respect the ovoid shape. This parameter is the ratio of the distance between the central point of the ellipse and its major axis length;
- Retinal thickness, the ROI (ILM/RPE) thickness should be bigger than $250\mu m$ equivalent to 64 pixels. This value corresponds to the normal size of the parafoveal region, (Goebel and Kretzchmar-Gross, 2002);
- The width of the candidate area should be inside a range of sizes [40 - 530]μm equivalent to [10 - 135] pixels. This way, the range ensures that the area of the candidates should be able to remove small artifacts and regions with a length that is approximately twice the normal of the retinal thickness.

Basically, the restrictions are based in terms of area, eccentricity, retinal layer thickness as well as the thickness between the specific retinal layers. As indicated before, the presence of CMEs leads to an increase of the retinal layers where the fluid is accumulated, and consequently, produce a global increment of the retinal tissue (ILM/RPE region).

As Fig. 8 shows, it is possible to conclude that the large majority of CMEs are within the ILM/OPL region. However, in more advanced pathological stages, they can also proliferate to the OPL/RPE region. In the outer region the contrast is lower, which makes the identification of the existing CMEs a more complex issue. In this case, we followed the same strategy as before, but adapting the parameters to the new conditions.

3 RESULTS AND DISCUSSION

As presented, the proposed system includes three different strategies to identify each ME type. All the strategies were tested using an image dataset that is composed by 50 OCT retinal images, centered in the macula, with a resolution of 2032×596 pixels. This dataset was acquired with a Spectralis® OCT confocal scanning laser ophthalmoscope from Heidelberg Engineering.

To ensure the efficiency of the system all the images were labeled by an expert clinician, identifying the location of the 3 types of MEs inside each scan. Based on this ground-truth, we constructed the training and testing sets for the DRT identification approach as well as validated the performance of SRD and CME identification approaches.

Precision, Recall and F-Measure were the used metrics for the validation of the proposed system, as indicated in Eqs.1, 2 and 3, respectively. The F-Measure is defined as a combination of both precision and recall metrics in a global measurement.

$$Precision = \frac{TP}{TP + FP} \qquad (1)$$

$$Recall = \frac{TP}{TP + FN} \qquad (2)$$

$$F - Measure = 2 * \frac{Precision * Recall}{Precision + Recall} \qquad (3)$$

where TP are the True Positives, FP the False Positives and FN the False Negatives.

Regarding the defined parameters, we used values that were empirically calculated, as it was previously mentioned in the methodology.

The efficiency of the proposed method for ME in OCT retinal images was evaluated according to quantitative metrics. As gold standard, for the SRD and CME cases, we measured if the central point of each detected edema was successfully identified, based on the specialist segmentation. Regarding the DRT case, we analyzed if each column was correctly identified when compared with the specialist opinion.

Regarding the case of SRD edemas, they are not as common as the others, affecting only a reduced groups of patients, as presented in (Otani et al., 1999). Moreover, when it is present, only one SRD pathological structure can be identified in each OCT scan. For that reason, the employed image dataset only contains 4 SRD edemas. The 4 cases were correctly identified by the proposed system.

For the DRT detection, the Naive Bayes classifier was trained using the proposed dataset with a 10 fold cross validation. Per each OCT image in the dataset, 80 samples were randomly selected, representing equally both DRT and non-DRT cases, resulting in a total of 4000 extracted samples.

Regarding the selected features using the SFS method, 4 of them were taken from the initial set: mean intensity, kurtosis, energy and energy from the GLCM matrix, as they include a high discriminant power to differentiate common retinal tissue patterns with respect to the DRT presence.

Using the selected features, the Naive Bayes classifier was trained and tested satisfactorily providing the presented metrics resulting in Table 2.

Table 2: Performance of the DRT detection approach.

Precision	Recall	F-Measure
84.04%	80.79%	83.35%

With this strategy, we were able to detect the 83.35% of the total regions of DRTs. The introduced mistakes are mainly derived from shadows that are produced by the presence of vessels but also from different pathological structures (hard-exudates). These shadows change the typical characteristics of the DRT edemas. Therefore, these artifacts lead to a miss-classification of the "sponge-region", decreasing the metric.

Regarding the CME case, it can be found in both regions (inner and outer retina), simultaneously. Therefore, the efficiency of the system with this ME type was tested in 2 phases, as listed in Table 3. In the first phase, the system was tested in the inner retina where the results were better. The F-Measure reaches a value of 87.48% in this case. The errors are mainly derived from missing CMEs with specific morphologies, as fusiform shapes and the presence of Microcystic Macular Edemas (MME). In the first case, cysts exhibit an unusual elongated shape, in the horizontal axis. Whereas, as a second case, the MMEs have a small area with a not well defined boundaries.
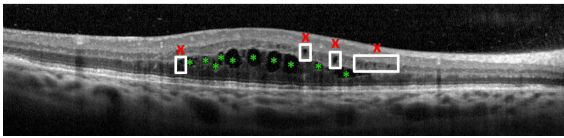
Figure 9: Example of OCT retinal image with undetected MMEs (x) and correct detections of CMEs (*).
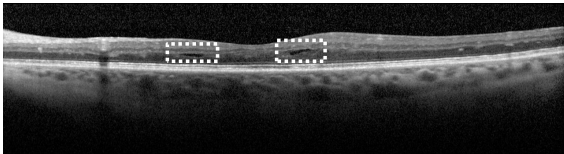

Figure 10: Example of the OCT retinal non detected CMEs (- -), due to the fusiform shape.

In the second phase, the method was tested in the outer retina where lower results were obtained given the higher complexity of the identification in this region. This decrease of the metrics is, as commented before, due to the fact that the almost absent contrast between the CME and the retina tissue. In a more complex scenario, the method is also able to detect efficiently the CMEs in the OPL/RPE region.

Figure 11 presents an illustrative result where the proposed system detects and characterizes the three types of ME even when they are simultaneously present on the same OCT image.

Table 3: Results of the quantitative metrics Precision, Recall and F-Measure for the CME detection.

Region	Precision	Recall	F-Measure
ILM/OPL	96.84%	78.34%	87.48%
OPL/RPE	88.26%	78.19%	74.40%
Both	89.98%	80.34%	81.95%

4 CONCLUSION

In this paper, we propose a novel automatic system that detects and characterizes the intraretinal fluid in the different types of ME using OCT retinal images. Using clinical criterions inspired in the Otani classification, the system automatically identifies and characterizes the ME in three types: SRD, DRT and CME. To do that, we analyzed intensity, texture, morphological and position properties of them retinal tissue to detect all the cases of each ME type. Regarding SRD and CME edemas, different approaches were implemented based on adaptive thresholding in specific regions of the retinal layers, as they usually present identifiable boundaries and a significant contrast with the retinal tissue. Then, to remove FPs, clinical conditions were applied based on the typical morphology
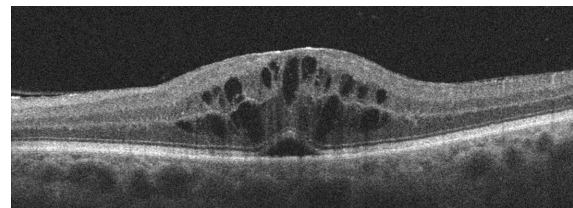
(a)
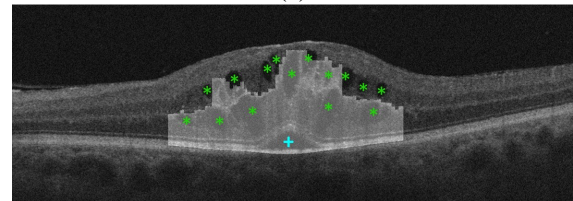
(b)

Figure 11: Example of an OCT retinal image with the detection of the three types of macular edema: SRD illustrated as (+), CME as (*) and DRT the selected columns.

of each type of ME. In the case of the DRT detection, a Naive Bayes classifier was trained to identify the regions where it is present using a list of 18 features as intensity, texture and domain knowledge properties. Then SFS is applied in order to select the ones with higher power of discrimination.

Experimental results show that the proposed system achieved promising results for the ME identification and characterization, even when they appear combined on the same retinal region. In particular, our system achieves a F-Measure of 83.35% for the DRT and 81.95% in the CME detection. While, in the detection of the SRD, the system detects all edemas that were present in the used dataset. Therefore, this system can be an important tool in clinical fields helping in the detection and characterization of retinal diseases.

As future works, the proposed system could have a larger dataset in order to reinforce the conclusions that were achieved in this work. Moreover, we aim the identification of more complex cases of the CME edemas. We also want to detect microcystic macular edema. For doing that, specific approaches can be designed with that purpose. Using the identified MEs, different statistic metrics can be derived as a way to provide valuable information to specialists and facilitate their diagnostic process. Therefore, it will be possible to motorize the disease evolution and increase the life quality of the patients.

ACKNOWLEDGEMENTS

REFERENCES

Alsaih, K., Lemaitre, G., Rastgoo, M., Massich, J., Sidibé, D., and Meriaudeau, F. (2017). Machine Learning Techniques for Diabetic Macular Edema (DME) Classification on SD-OCT Images. *Biomed. Eng. Online*, 16(1):68.

Baamonde, S., de Moura, J., Novo, J., and Ortega, M. (2017). Automatic Detection of Epiretinal Membrane in OCT Images by Means of Local Luminosity Patterns. In *International Work-Conference on Artificial Neural Networks*, pages 222–235. Springer.

Carmona, L. and Hernández, F. (2015). Revisión Bibliográfica: Edema Macular Diabético, Repercusiones y Tratamiento. *Revista Médica del Instituto Mexicano del Seguro Social*, 53(5):600–607.

Chiu, S., Li, X., Nicholas, P., Toth, C., Izatt, J., and Farsiu, S. (2010). Automatic Segmentation of Seven Retinal Layers in SDOCT Images Congruent with Expert Manual Segmentation. *Opt. Express*, 18(18):19413–19428.

de Moura, J., Novo, J., Rouco, J., Penedo, M., and Ortega, M. (2017). Automatic Identification of Intraretinal Cystoid Regions in Optical Coherence Tomography. In *Conference on Artificial Intelligence in Medicine in Europe*, pages 305–315. Springer.

Dijkstra, E. (1959). A Note on Two Problems in Connexion with Graphs. *Numerische Mathematik*, 1(1):269.

Gelfand, J., Nolan, R., Schwartz, D., Graves, J., and Green, A. (2012). Microcystic Macular Oedema in Multiple Sclerosis is Associated with Disease Severity. *Brain*, 135(6):1786–1793.

Goebel, W. and Kretzchmar-Gross, T. (2002). Retinal Thickness in Diabetic Retinopathy: A Study Using Optical Coherence Tomography (OCT). *Retina*, 22(6):759–767.

González, A., Remeseiro, B., Ortega, M., Penedo, M., and Charlón, P. (2013). Automatic Cyst Detection in OCT Retinal Images Combining Region Flooding and Texture Analysis. In *CBMS, 2013 IEEE 26th International Symposium on*, pages 397–400. IEEE.

Gupta, A., Raman, R., Mohana, K., Kulothungan, V., and Sharma, T. (2013). Communications Between Intra-retinal and Subretinal Space on Optical Coherence Tomography of Neurosensory Retinal Detachment in Diabetic Macular Edema. *Oman J.of Ophthalmol.*, 6(3):183.

Helmy, Y. and Allah, H. (2013). Optical Coherence Tomography Classification of Diabetic Cystoid Macular Edema. *Clin. Ophthalmol.*, 7:1731.

Joussen, A., Gardner, T., Kirchhof, B., and Ryan, S. (2010). *Retinal Vascular Disease*. Springer Science & Business Media.

Montuoro, A., Waldstein, S., Gerendas, B., Schmidt-Erfurth, U., and Bogunović, H. (2017). Joint Retinal Layer and Fluid Segmentation in OCT Scans of Eyes with Severe Macular Edema Using Unsupervised Representation and Auto-Context. *Biomed. Opt. Express*, 8(3):1874–1888.

Noma, H., Funatsu, H., Mimura, T., and Shimada, K. (2011). Visual Function and Serous Retinal Detachment in Patients with Branch Retinal Vein Occlusion and Macular Edema: A Case Series. *BMC Ophthalmology*, 11(1):29.

Ooto, S., Tsujikawa, A., Mori, S., Tamura, H., Yamashiro, K., and Yoshimura, N. (2010). Thickness of Photoreceptor Layers in Polypoidal Choroidal Vasculopathy and Central Serous Chorioretinopathy. *Graefe's Arch. Clin. and Exp. Ophthalmol.*, 248(8):1077–1086.

Otani, T., Kishi, S., and Maruyama, Y. (1999). Patterns of Diabetic Macular Edema with Optical Coherence Tomography. *Am. J. of Ophthalmol.*, 127(6):688–693.

Otsu, N. (1979). A Threshold Selection Method from Gray-Level Histograms. *EEE Trans. Syst. Man. Cybern B. Cybern.*, 9(1):62–66.

Panozzo, G., Parolini, B., Gusson, E., Mercanti, A., Pinackatt, S., Bertoldo, G., and Pignatto, S. (2004). Diabetic Macular Edema: An OCT-Based Classification. In *Seminars in Ophthalmology*, volume 19, pages 13–20. Taylor & Francis.

Sidibé, D., Sankar, S., Lemaître, G., Rastgoo, M., Massich, J., Cheung, C., Tan, G., Milea, et al. (2017). An Anomaly Detection Approach for the Identification of DME Patients Using Spectral Domain Optical Coherence Tomography Images. *Comput. Methods and Programs in Biomed.*, 139:109–117.

Trichonas, G. and Kaiser, P. (2014). Optical Coherence Tomography Imaging of Macular Oedema. *Br. J. of Ophthalmol.*, 98(Suppl 2):ii24–ii29.

WHO (2012). Global Data on Visual Impairments 2010. *Geneva: World Health Organ.*

Willoughby, A., Chiu, S., Silverman, R., Farsiu, S., Bailey, C., Wiley, H., Ferris, F., and Jaffe, G. (2017). Platform-Independent Cirrus and Spectralis Thickness Measurements in Eyes with Diabetic Macular Edema Using Fully Automated Software. *Transl. Vis. Sci. & Technol.*, 6(1):9–9.

Wolff, B., Azar, G., Vasseur, V., Sahel, J.-A., Vignal, C., and Mauget-Faÿsse, M. (2014). Microcystic Changes in the Retinal Internal Nuclear Layer Associated with Optic Atrophy: a Prospective Study. *J. Ophthalmol.*, 2014.

Zhu, S. and Yuille, A. (1996). Region Competition: Unifying Snakes, Region Growing, and bayes/MDL for Multiband Image Segmentation. *IEEE Trans.s on Pattern Anal. and Mach. Intell.*, 18(9):884–900.